SOME THEORETICAL WALL-INTERFERENCE CALCULATIONS IN SLOTTED TRANSONIC TEST-SECTIONS, THREE-DIMENSIONAL FLOWS

Y. C-J. Sedin and K. R. Karlsson
Saab-Scania, Linköping, Sweden

Abstract

Transonic wall-interference is numerically simulated for flows as typically set up by slender wings at angles of attack in slotted test-sections.

A filtered small disturbance velocity potential is iteratively solved between the wall and an inner interference shell, enclosing the model. In doing so an inviscid slot flow theory is repeatedly applied as an outer wall condition. A number of cases for which model size, slot geometry and plenum pressure are varied have been calculated. The slots are unformly distributed and of constant width. Typical pressure distributions and interference numbers are illustrated.

This work is an extension of previous numerical efforts on symmetric flows to incorporate also asymmetric flows into the wall condition.

Nomenclature

ALFA = angle of attack
a = slot width
AR = $4b^2/S$, wing aspect ratio
b = wing half-span
c = wing root chord
C_L = $L/(\rho_\infty U_\infty^2 S)/2$, lift coefficient
C_D = $D/(\rho_\infty U_\infty^2 S)/2$, drag coefficient
C_p = $(p-p_\infty)/(\rho_\infty U_\infty^2)/2$, pressure coefficient
D = drag force
$\mathcal{F}$ = wall b.c. functional, Eq(1)
FTIL = figure of tunnel interference-lift, Eq(8)
FTID = figure of tunnel interference-drag, Eq(8)
FTIP = figure of tunnel interference-pressure, Eq(8)
FTIR = $\sqrt{FTIL^2+FTID^2}$
f(x,θ) = $\bar{\varphi}_r(x,b,\theta)$, inner b.c., Eq(3)
HSP = short hand for half-span (=b)
H^{ik} = slot cross-flow influence coefficient matrix, Ref 1
L = lift force
l = slot depth, Fig 2
M_∞ = Mach number of reference flow
M_0 = $M_\infty\sqrt{1-(\gamma+1)\delta}$, entrance Mach number
N = number of slots
p = pressure
P = circumferential slot width parameter, Fig 12
p_p = pressure in plenum chamber
p_∞ = pressure in freestream reference flow
q = slot volume flux/unit length, Eq(5)
Q = normalized slot flow potential, Ref 1
s = local half-span of wing
S = wing area
r = radius vector in crossflow plane (r=1 at tunnel wall)
U_∞ = velocity in freestream reference flow
VENT = total tunnel wall ventilation, %
v = normalized slot flow velocity at y_p, Ref 1
x = distance along tunnel axis
x_0 = slot start, upstream boundary of computational domain
x_1 = downstream end of computational domain
y_p = coordinate of line in slot centerplane where the plenum pressure is imposed, Figs 2 and 3
y_{p0} = y_p in the "jet region", Fig 3
α = wing angle of attack
β = $\sqrt{1-M_\infty^2}$
γ = specific heat ratio (=1.4)
δ = $(p_p-p_\infty)/\rho_\infty U_\infty^2$ normalized plenum pressure
ρ = perturbation velocity potential to "exact" problem
$\bar{\varphi}$ = perturbation velocity potential to approximate (filtered) problem, Eq(2)
$\bar{\varphi}_0$ = integration constant given at beginning of slot, Eq(5)
ν = highest order of harmonic analysis of interference
ρ_∞ = density of freestream reference flow
θ = circumferential cylinder coordinate
i,k = superscripts, Eq(5)
$(\ )_x$ = $\partial/\partial x$, derivation with respect to x
$(\ )_r$ = $\partial/\partial r$, derivation with respect to r
$(\ )_\theta$ = $\partial/\partial\theta$, derivation with respect to θ

1. General introduction

Wall interference in wind-tunnel test sections is a serious and complicated problem when testing models at transonic speeds. One way to decrease this interference is to ventilate the walls through a number of longitudinal slots.

In Ref 1 Berndt formulated an inviscid theory of wall interference in slotted transonic test sections. Later Karlsson and Sedin[2,3] numerically applied this theory to axisymmetric bodies at zero angle of attack in cylindrical test sections with uniformly distributed slots. In Ref 3, the inverse problem of finding slot shapes yielding no or neglible interference on the model was adressed and a procedure to create such slots was also demonstrated. In these investigations the displacement effects of the wall boundary layer turned out to be an important component.

The gradient of the displacement thickness gives rise to an increased crossflow through the slots contributing to the pressure difference between the plenum chamber and the wall. This phenomenon is of course more pronounced in transonic flow where lateral interactions are very stiff. Hence, even in an empty tunnel there might appear quite a substantial inflow into the slots especially at the beginning if they are started from zero slot width. Studies about these problems are currently under way supported by experiments carried out by Sörensén and Nedersjö[4] at the Aeronautical Research Institute of Sweden (FFA). Some of these activities have been reviewed by Berndt[5].

Up to now, the numerical efforts (Ref 2-3) of computing slotted wall interference have been focused mainly upon axisymmetric bodies at zero angle of attack. However, a more difficult and important

matter is of course to see how things are going for a wing at an angle of attack, where the flow disturbances are large due to the asymmetric flow situation. The present paper is a report on the first attempts to numerically apply the theory of Ref 1 to some simple three-dimensional flow fields typically set up by a slender wing at an angle of attack. To simplify matters and to concentrate on the phenomenological consequences of the theory (Ref 1), the calculations are limited to the flow between two concentric cylinders. The inner boundary is given a radial outflow condition obtained from a line doublet placed along the centerline of the test section. The strength of this doublet line is related to that of a slender delta wing at an angle of attack. The field between the cylinders is governed by a transonic non-linear small disturbance potential flow equation. No boundary layer effects are treated in these investigations. Moreover, the slot widths in the streamwise direction are assumed constant.

2. Notes on the theoretical and computational backgrounds

The wall theory of Ref 1 is inviscid and built on the derivation of an approximate velocity perturbation potential $\bar{\varphi}$. Compared to the "exact" solution φ, the approximate $\bar{\varphi}$ is created by averaging (filtering) φ with respect to higher order cross-flow variations caused by the slots and the walls. However, by using "slender-body" cross-flow theory in combination with matched asymptotic expansions, the details of the slot flow is coupled to the filtered potential through a pressure balance equation for each slot. A wall boundary condition then results at the position of each slot giving a relation between $\bar{\varphi}$ and the radial velocity $\bar{\varphi}_r$ there. This is here interpreted through the functional $\mathcal{F}$:

$$\bar{\varphi} = \mathcal{F}(\bar{\varphi}_r) \qquad (1)$$

In three dimensions a trigonometric interpolation is needed between the slots to get a complete description of $\bar{\varphi}$ at the wall as a function of the circumferential coordinate. The functional $\mathcal{F}$ includes the dependence on geometrical slot data as well as the plenum pressure and the number of slots. In principle relation (1) symbolizes a system of ordinary differential equations that has to be solved simultaneously including the position of the plenum pressure surface for each slot. Once the approximate problem of $\bar{\varphi}$ is solved it is possible to calculate the "exact" φ at the wall to evaluate the wall pressure. Close to the model in the centre of the tunnel $\bar{\varphi}$ is equivalent to φ.

At the inner boundary radial out-flow conditions $\bar{\rho}_r$ are prescribed. These conditions are here generated by a typical three-dimensional line doublet obtained from linear theory by regarding the asymptotic far field from a mathematically thin and slender delta wing at an angle of attack in an infinite freeair stream. The inner cylindrical boundary has a diameter equal to the span of the wing, thus enclosing the wing.

To define some measures of wall interference two different cases are solved one for the reference freestream and one for the tunnel case. In both cases the same inner boundary conditions ($\bar{\varphi}_r$) are imposed. The interference is evaluated at the inner boundary (interference shell) by means of some relative measures called Figures of Tunnel Interference (FTI-), approximately referring to lift (FTIL), drag (FTID) and pressure (FTIP). As the wake representation (line doublet) is not moved by the wall influence in the present calculations the FTI-values are evaluated over that part of the inner boundary that covers the length of the wing only.

Concerning the upstream inflow condition for the tunnel case, $\bar{\varphi}_x$ is set corresponding to the plenum pressure. This effectively connects the inflow Mach number to the plenum pressure defining the rule between the inflow Mach number and the plenum pressure. This chosen rule will of course not always guarantee a smooth inflow matched to the interior of the computational domain especially not if the disburbances from a large model propagate that far upstream (see Ref 3). However, in the present applications the models do not disturb the inflow part of the test section and the slot widths are assumed constant surpressing latent physical and mathematical difficulties with slots gradually starting from zero slot width. No wall boundary layers are treated in this study.

3. Equations and Computational Procedures

The field equation to be solved between the inner boundary (interference shell, r=b) and the tunnel wall (r=1) is the small perturbation equation given by

$$(1-M_\infty^2-M_\infty^2(\gamma+1)\bar{\varphi}_x)\bar{\varphi}_{xx}+(r\bar{\varphi}_r)_r/r+\bar{\varphi}_{\theta\theta}/r^2=0 \qquad (2)$$

(x,r,θ) is a cylindrical coordinate system with x pointing downstream. M_∞ is the freestream Mach number of the desired nominal reference flow, which the numerical tunnel run is supposed to simulate as closely as possible in the neighbourhood of the model. The potential $\bar{\varphi}$ is the filtered potential that is equal to or close to the "exact" solution φ in the interior of the test section. In Ref (6) a rapid finite difference method was exploited for solving transonic flow problems in cylindrical coordinates and this method has here been applied to Eq (2). However, any other convenient method could have been used, of course.

Now, concerning the boundary conditions to Eq (2) they are as follow:

$$\begin{aligned}
&\text{Inner, } r=b: \quad \bar{\varphi}_r=f(x,\theta), \text{ given line doublet}\\
&\text{Outer, } r=1: \bar{\varphi}=\mathcal{F}[\bar{\varphi}_r(x,1,\theta)], \text{ wall condition}\\
&\text{Upstream, } x=x_0: \quad \bar{\varphi}_x=-\delta, \text{ entrance Mach No}\\
&\text{Downstream, } x=x_1: \ \bar{\varphi}_{xx}=0, \text{ no acceleration.}
\end{aligned} \qquad (3)$$

The function $f(x,\theta)$ defining the inner boundary condition is typically derived by regarding a line doublet solution to Eq (2) neglecting the non-linear term. The strength of the line doublet is found by matching the outer three-dimensional doublet solution to the inner slender-body cross-flow about a slender delta wing at an angle of attack α. The disturbance potential of the linear line doublet then comes out to be

$$\bar{\varphi}(x,r,\theta) = \frac{1}{2}\alpha\cdot\frac{\sin\theta}{r}\cdot\int_{-c/2}^{\infty} K(x-\xi;\beta^2 r^2)\cdot s^2(\xi)\,d\xi$$

$$K(x-\xi;r^2\beta^2) = \frac{1}{2}\beta r^2\,[x-\xi)^2+\beta^2 r^2]^{-2/3}$$

Here denotes α the angle of attack, while $\beta^2=(1-M_\infty^2)$ and s is the local half-span of the wing. The half-span at the trailing edge is b while c is the root chord. All calculations have been carried out with a wing aspect ratio of AR=2.5 giving c in terms of b. The wing is placed with its apex at x=-c/2. The radial outflow at r=b, derived from Eq (4), is kept the same for both the nominal freeair reference flow and the simulated tunnel case when evaluating the wall-interference at the half-span radius, r=b. The computational field model is as sketched in Fig 1, where the computational domain for Eq (2) is within $b \le r \le 1$, $x_0 \le x \le x_1$.

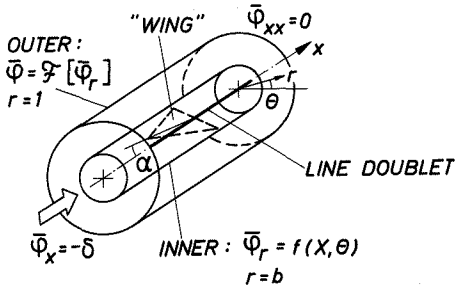

Fig 1. Computational model

Turning to the outer wall condition, Eq (1), this is a bit more complicated in three dimensions compared to the axisymmetric case solved in Refs 2-3. However, for constant slot width (denoted by a) Eq (1) is equivalent to the following coupled system for the slots

$$\sum_{i=1}^{N}\left\{\frac{1}{2}+\sum_{j=1}^{\nu}\cos[j(\theta^k-\theta^i)]\right\}q^i = \pi\cdot\bar{\varphi}_r(x,1,\theta^k),$$

$$dy_p^k/dx = q^k v/a^k, \qquad (5)$$

$$d/dx[\bar{\varphi}(x,1,\theta^k)-\bar{\varphi}_0(x_0,1,\theta^k)+(Q-\pi^{-1}\ln a^k)q^k + \sum_{i=1}^{N} H^{ik}q^i] + (q^k v/a^k)^2/2 + \delta^k = 0$$

The superscript k ($1 \le k \le N$) indicates the slot considered while superscript i denotes a running slot index and ν, ($2\nu+1 \le N$), is the picked order of the trigonometric interpolation (expansion) polynomial.

Now, looking at the physical phenomena behind Eq (5), the first equation is the cross-flow continuity equation determining the slot volume fluxes q^i per unit length through the slots. The second equation constitutes a kinematic tracing of the plenum pressure surface y_p^k along which the normalized plenum pressure coefficient δ^k is imposed. The last equation is the pressure balance equation at the surface y_p^k for slot number k and from this equation the filtered $\bar{\varphi}(x,1,\theta^k)$ can be integrated, implicitly in terms of $\bar{\varphi}_r(x,1,\theta^i)$ via q^i. Thus, the functional relationship of Eq (1) is formulated. The variables v and Q are normalized velocity and velocity potential functions for an isolated slot of unit width and unit flux per unit length. H^{ik} are elements of an influence coefficient matrix of the far distant wall and slot interaction on the considered slot k. $\bar{\varphi}_0$ is an integration constant. For more details of the slot flow functions, see Refs 1,3. Before leaving the outer wall condition it should be pointed out that with uniformly distributed slots, as in the present paper, the slot flux equations of system Eqs (5) are simplified according to

$$q^k = 2\pi\,\bar{\varphi}_r(x,1,\theta^k)/N$$

Concerning the numerical solution of Eq (2) with conditions (3) this is carried out in very much the same way as was reported on in the axisymmetric case, Ref 3. That is to say an iterative process is established in the computational domain by reapetedly changing the outer (r=b) wall condition of $\bar{\varphi}$ after every interior field sweep. This results in a continous updating of $\bar{\varphi}$ via $\bar{\varphi}_r$ at r=b, $\theta=\theta^k$. As was already observed in Ref 3 the corrections in the outer boundary condition had to be heavily under-relaxed from one iteration to another to get a convergent procedure. To obtain a complete circumferential outer description of $\bar{\varphi}(x,1,\theta)$ in the computational finite-difference grid a trigonometric interpolation of order ν ($2\nu+1<N$) has to be done from values $\bar{\varphi}(x,1,\theta^k)$ obtained at slot positions θ^k. If $2\nu+1<N$, a least square fit has to be applied.

The details of the slot flow model will not be repeated here but are as schematically shown in Fig 2-3.

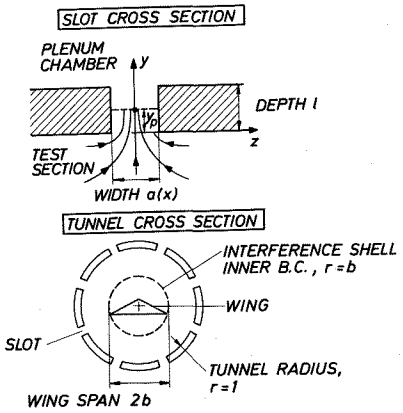

Fig 2. Slot and tunnel cross sections

Figure 3, reproduced from Ref 3, shows an assumed flow situation of a particular slot. Fast air is entering the slot in region I penetrating the plenum chamber as a jet in region II, while regions III and IV indicate a return of fast air. The cross-hatched line y_p is the plenum pressure surface, which is a free surface in regions I, III and IV. The numerical modelling of the wall condition Eq(5) and the interpretation of this in connection to

Fig 3 is the same as that of Ref 3 and will not be reviewed here.

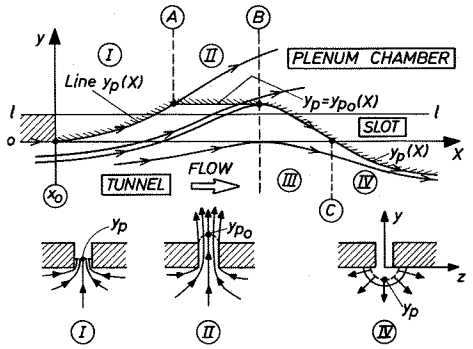

Fig 3. Slot flow model

To analyze the wall pressure the filtered solution $\bar{\varphi}$ is matched to the "exact" solution φ in the neighhourhood of the wall. According to Ref 1 this will result in the following potential φ_w at the wall position θ_w, r=1.

$$\varphi_w=\bar{\varphi}_w-\pi^{-1}\sum_{i=1}^{N} q^i\left\{\ln r_w^i+\sum_{j=1}^{\nu} j^{-1}\cdot\cos[j(\theta_w-\theta^i)]\right\} \tag{6}$$

$$r_w^i = 2^{1/2}\,[1-\cos(\theta_w-\theta^i)]^{1/2}$$

The wall pressure then is $c_p=-2\varphi_{wx}$. The approximation of the pressure coefficient along the inner interference shell (r=b) is

$$C_p = -2\bar{\varphi}_x - \bar{\varphi}_r^{\,2} \tag{7}$$

The tunnel interference is numerically quantified in qualitative numbers called figures of tunnel interference (FTI) with approximate reference to pressure (FTIP), lift (FTIL) and drag (FTID). These numbers are evaluated at the inner boundary (r=b) according to

$$\text{FTIP} = \Big[\sum_{n=1}^{n}\Delta C_{p_i}^{\,2}/n\Big]^{1/2} / |C'_{p_{min}}|$$

$$\text{FTIL} = \sum_{i=1}^{n}(\Delta C_{p_i}\sin\theta)/\sum_{i=1}^{n}(C'_{p_i}\cdot\sin\theta_i) \tag{8}$$

$$\text{FTID} = \sum_{i=1}^{n}(\Delta C_{p_i}\cdot\bar{\varphi}_{r_i})/\sum_{i=1}^{n}(C'_{p_i}\cdot\bar{\varphi}_{r_i})$$

ΔC_{p_i} is the pressure coefficient difference between the tunnel and the desired freeair reference case, the difference being evaluated at mesh point i. The symbol n is the number of mesh points covering the root chord of the delta wing. $|C'_{p_{min}}|$ is the absolute value of the most negative (suction) pressure coefficient over the wing in the nominal freeair reference case. Primed C_p-values (C'_p) indicate data from the freeair reference flow. As the computational grid is equidistant in x and θ directions, the differential areas of the inner cylinder is the same all over the wing so these areas are eliminated and thus absent in the ratios defining FTIL and FTID.

To compare calculated slotted wall-interference with simple linear cross-flow theory for closed wall sections a qualitative formula for the latter will be derived. Though the theory of Ref 1 is singular in the limit of zero ventilation, it could be interesting to compare this at about 1-3 % ventilation to closed wall theory. To this end, regard the two-dimensional cross-flow at the wing trailing edge. Put in two counter-rotating trailing vortices, one at each wing tip mirror reflecting them in the circular closed wall tunnel. Choose the wing collocation points for fulfilling the tangent flow condition due to α at the span stations $\pm b/\sqrt{2}$. With this choice the calculated vortices will give the classical slender-body lift curve slope ($C_{L_\alpha}=\pi\cdot(AR)/2$) in the limit $b\to 0$, AR=const. Then, the following wall-interference at constant angle of attack comes out for the lift coefficient C_L in a circular closed wall test section

$$(C_L-C_L')/C_L' = \tfrac{1}{2}b^2/(1-b^2) \tag{9}$$

Here C_L' is the freeair value. The same approximate expression as Eq(9) will be found for the induced drag when the induced downwash angle ($\alpha/2$) at the collocation points is picked for the half-infinite trailing line-vortex system.

Another nearby theoretical limit that could be checked upon is the case of an open jet (100 % ventilation). However, this case is a bit more complicated to treat theoretically and will not be considered here. It is known that an open jet usually gives a negative wall-interference contribution to the lift and drag coefficients. Eq(9), however, shows a positive increase in these forces due to the closed wall interference. From calculated slotted wall data it will be seen that a cross-over from negative to positive interference really exists at quite common values of wall ventilation.

4. Calculated Results

No attempts are here made to find optimal strategies for minimizing wall-interference or correcting wind-tunnel data. Instead some numerical investigation are carried out to see the consequences of the theory with reference to slot geometry and model size. In all calculations the delta wing that generates the inner boundary condition has an aspect ratio of 2.5. The unit of length is the tunnel radius in all figures.

In principle, the presented results are divided into two parts. One part shows details of pressure and slot flow distributions (Figs 4-10). The second part illustrates compiled wall-interference data (Figs 11-17) in terms of interference numbers viz slot and model geometry parameters.

Figures 4-10 are computer plotted. Due to this all variables are explicitly expressed in capital letters. A symbol indicating the angular position θ at which the considered graphs are recorded is also shown in these figures. Noted Mach numbers are always referring to M_∞ of the nominal freeair reference flow.

The finite difference grids for solving Eq(2) have been equidistant in x and θ-directions but streched in the radial direction. The freeair cases have typically been solved in a grid with (101x61x11)

points in x, r and θ directions respectively. The outer boundaries are then placed far off from the wing, the outer radius typically 6-7 semi-spans away. Two different step lengths in x have been used covering the wing with 17 or 9 points respectively. The grids in the tunnel cases have simply been cut out from the freeair cases retaining the same nodes. The iterations have been stopped when the maximum potential correction has reached values of about 10^{-5}-10^{-6}. This usually occurs after about 50 - 100 field iterations back and forth in the manner of the method described in Ref(6).

5. Comments on the numerical results

Fig 4 shows pressure distributions along the inner interference shell above ($\theta=90^{o}$) and below ($\theta-90^{o}$) the wing at $M_{\infty}=0.95$ and at a high angle of attack attitude of $\alpha=13.1^{o}$. The number of slots is 8 and the total wall ventilation 9.2 %. As can be seen from the pressure graphs this example gives a very strong interference situation. Paradoxally, however, the interference on the lift force (FTIL= -0.03) is quite small though the local pressure and Mach number distributions above and below the wing are not being correct. A strong shock-wave is shown above the wing in the freeair reference case compared to a relatively mild compression apparent in the tunnel case. Generally there is a slow down in tunnel speed at the wing position. One measure to partly compensate for this would be to apply some amount of plenum suction ($\delta<0$), though this would act all the way up to the entrance section too. An estimated C_L-value in the case of Fig 4 is in the order of 0.9.

In Fig 5 the angle of attack is decreased to 6.6^{o} compared to that of Fig 4. The main relative features of the pressure distributions are roughly unchanged in comparison to Fig 4 and the wall-interference on lift and drag is still negative and not too far away from that of Fig 4. However, the interference on drag is larger and more pronounced in Fig 4 probably due to more transonic flow in that case. The latter, of course, also rises the question whether second order cross-flow terms should be implemented in the field equation at high angles of attack. Such terms in the inner field can create net streamline displacement areas in the outer as was pointed out by Cheng and Hafez[7]. The order of C_L in Fig 5 is about 0.45.

One safe way to reduce the wall-interference is of course to reduce the model size which is being demonstrated in Fig 6. The wing semi-span is here only 25 % of the tunnel radius. For this model size and angle of attack the wall-interference is almost neglible and the pressure distributions agree very well with the desired freeair reference flow. Contrary to Fig 6 an increase in model size is shown in Fig 7. The wing half-span is here 65 % of the tunnel radius. Paradoxally once again, in spite of the large model, the interference on lift and drag forces is small but the pressure distributions at the inner boundary are far away from the nominal freeair reference flow giving incorrect Mach number distributions at the wing.

Fig 8 shows a similar situation to that of Fig 5 though in the present case a small amount of plenum pressure suction has been applied giving an entrance Mach number of $M_{o}=0.96$. As can be seen from the pressure graphs the pressure peaks above and below the wing now agree fairly well with the described freeair reference flow. However, the increased tunnel speed then manifests itself in different pressure gradients at the model. Reducing the plenum pressure to half of the applied suction in Fig 8 would have given a better overall pressure agreement as is illustrated by Fig 14.

Figures 9a-9d give a complete picture of pressure and slot flow data for a case where the plenum suction is half of that used in Fig 8 and the Mach number is reduced to $M_{\infty}=0.90$. The wall-interference on the lift and drag forces are here less than 1 % while the overall influence on pressure gives a value FTIP=0.06, the smallest calculated for this model size. Figures 9a-9b show pressures on the interference shell and the wall, while Fig 9c shows the filtered radial outflow velocity $\bar{\varphi}_r$ at the wall. Apparently there is an inflow from the plenum chamber at the tunnel ceiling while an outflow is indicated at the bottom. It is also interesting to see how an outflow is recorded also at the side wall, $\theta=0$. Figure 9d shows the plenum pressure surfaces y_p and confirms the physical behaviour of Fig 9c. Moreover, it can be seen how the bottom slots are filled up with fast air and how the plenum pressure surface y_{p_o} in the "jet region" (see Fig 3) is reached downstream of the wing for the bottom slots.

Fig 10 is in principle the same case as that of Fig 9 except for a doubling of the number of slots to N=16 while keeping the total ventilation the same (9.2 %). Though the crossflow velocities in the slots intuitively could have been expected to be about the same as those of Fig 9 the interference situation gets much worser in the case with 16 slots.

Figures 11-17 show some compiled interference data with respect to varying slot and model size geometries as well as changing plenum pressures.

Fig 11 displays wall-interference numbers in terms of FTIL, FTID and FTIP as functions of tunnel wall ventilation. The limits from linear wall-interference theory is here confirmed in the meaning that increased forces (C_L, C_D) are obtained for small ventilations while more open tunnels give smaller forces. The cross-over point of zero wall-interference for C_L and C_D is here reached at about 7 % wall ventilation. The computed FTIL and FTID data roughly reach the closed wall theory of Eq(9) at about 1-3 % of tunnel ventilation.

Looking at the different interference numbers one could say that FTIP should be the most stringent measure of wall interference as this has got an immediate impact on boundary layer developments and compressibility effects on e.g. pitching moment characteristics and so forth. Then it is disappointing to see in Fig 11 how FTIP has got quite large values at the same time as FTIL and FTID obtain their zero values at about 7 % ventilation. Not even the minimum value of FTIP=0.09 at 15 % ventilation is especially impressive regarding the disagreement in pressure and Mach number distributions this would result in. The situation can be improved, however, as shown in Fig 14 by applying some plenum pressure suction, thus slightly increasing the entrance Mach number M_{o} above M_{∞}. However, it will still be doubtful whether such actions can give FTIP-values small enough to be regarded as being interference-free

situations would be to try the optimal slot shape design procedure as developed for axisymmetric bodies in Ref 3.

Fig 12 shows what happens when the slot widths are sinusoidially varied in the angular (θ) direction at constant total wall ventilation. From this it turns out that the force-interference can be diminished by slightly closing the bottom slots and correspondingly opening up the slots at the tunnel ceiling.

Fig 13 displays interference numbers as functions of angle of attack. FTIL and FTID are strongly diverging from each other at high angles of attack a phenomenon probably due to the non-linear term of Eq(2). The filled symbols indicate calculations with a coarser grid system.

Fig 14 shows what was mentioned before, namely that the wall-interference can be reduced by applying some plenum suction increasing the tunnel air speed. The reduction in FTIP is almost 50 % by lowering the plenum pressure from C_p=0 to C_p=-0.010 thus increasing the entrance Mach number from 0.95 to about 0.96.

Fig 15 illustrates wall-interference due to variations in model size. For this tunnel setting the wing span should not exceed about 25 % of the tunnel diameter for having an almost interference-free situation. Moreover it is demonstrated that a slotted tunnel is superior to a closed wall tunnel as represented by Eq(9).

Fig 16 shows the influence by variations in the reference Mach number. Obviously for this model and tunnel setting the interference is smallest at subcritical Mach numbers. Fig 17 displays the influence by the slot depth parameter. Within the calculated range $0.5 \leq l/a \leq 1.5$ the slot depth does not seem to be too critical a parameter, though values of $1 \leq l/a \leq 1.5$ are beneficial with reference to FTIL and FTID in this case.

6. Concluding remarks

A numerical investigation has been made to see the consequences of a transonic wall interference theory for slotted test-sections with reference to asymmetric flows as typically generated by slender wings at angles of attack. Results have been obtained for various slot geometries and model sizes. The numerical results seem to be compatible with what could have been expected from physical points of views.

The problem of finding strategies for minimum wall-interference is outside the scope of this paper. However thus far by experience, it seems to be difficult to achieve neglible interference with respect to pressure for models large enough to give practically acceptable model Reynolds numbers. If the present temporary restriction of having constant slot widths in the calculations is to be blamed for this, remains to be seen. So far, some hope could be set to the optimum slot shape design procedure of Ref 3. However, this has to be tested first on lifting wings before any definite answers can be given to this.

References

1. Berndt, S.B., "Inviscid theory of wall interference in slotted test sections," AIAA journal Vol 15, Sept 1977, pp 1278-1287.

2. Karlsson, K.R. and Sedin, Y.C-J., "Axisymmetric calculations of transonic wind tunnel interference in slotted test sections," AIAA Journal Vol 17, Aug 1979, pp 917-919.

3. Karlsson, K.R. and Sedin, Y.C-J., "Numerical design and analysis of optimal slot shapes for transonic test sections - Axisymmetric flows," Journal of Aircraft, Vol 18, March 1981, pp 168-175.

4. Sörensén, H. and Nedersjö, S.E., "Vägginterferensmätningar med stora modeller och olika spaltformer," (Wall-interference measurements of large models and different slot shapes.) Data not published. Private communications, Nov 1980.

5. Berndt, S.B., "Flow properties of slotted-wall test sections," Paper No 6, Agard Specialist Meeting on Wall Interference in Wind Tunnels, London, May 19-20 1982.

6. Karlsson, K.R. and Sedin, Y.C-J., "The method of decomposition applied in transonic flow calculations," Lecture Notes in Physics, Vol 59, Springer Verlag, New York, 1976, pp 262-267.

7. Cheng, H.K. and Hafez, M.M., "Transonic equivalence rule; a nonlinear problem involving lift," J. Fluid Mech. (1975), vol 72, pp 161-187.

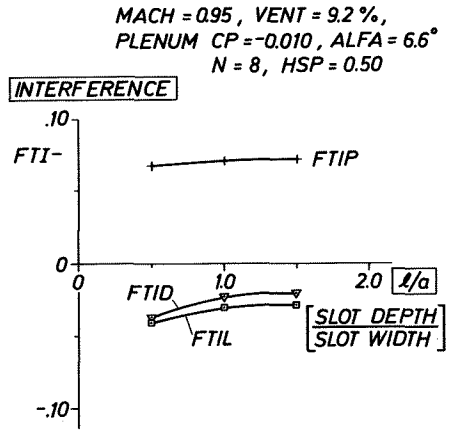

Fig 17. Slot depth influence on wall-interference.

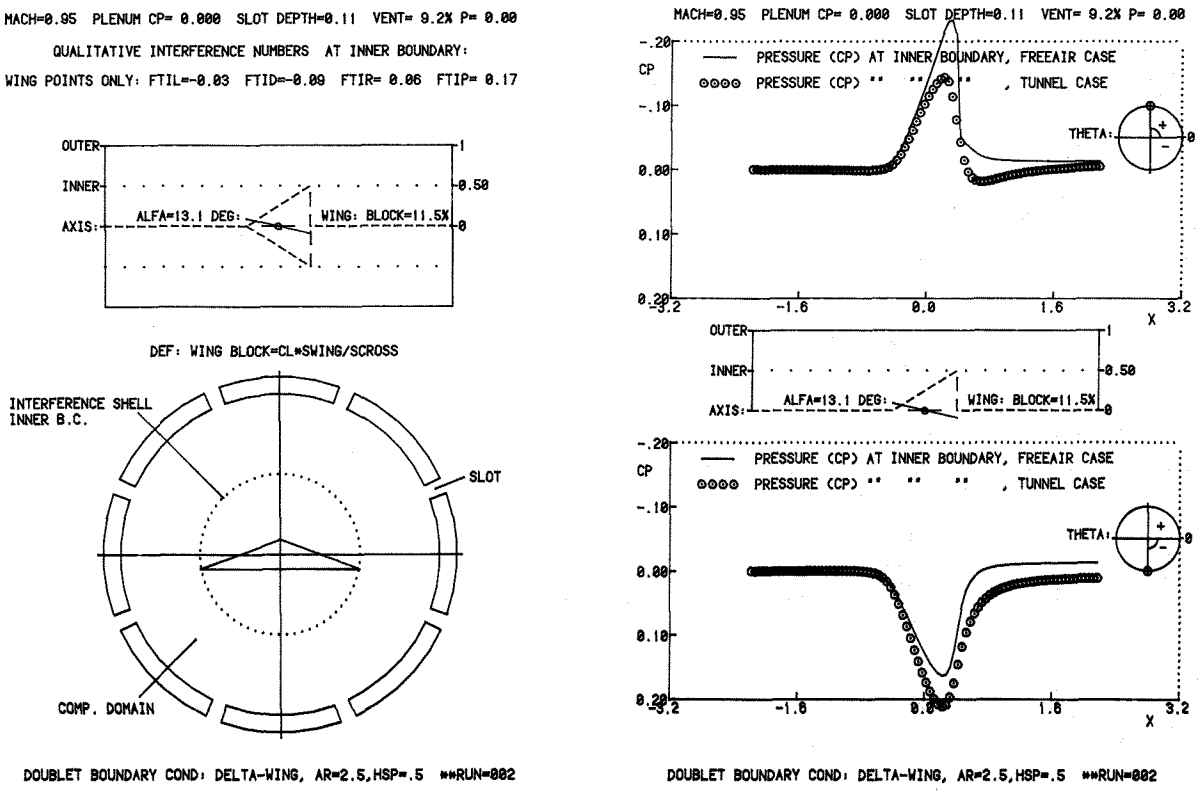

Fig 4. Pressure distributions at inner boundary of a tunnel case at M_∞=0.95, α=13.1°.

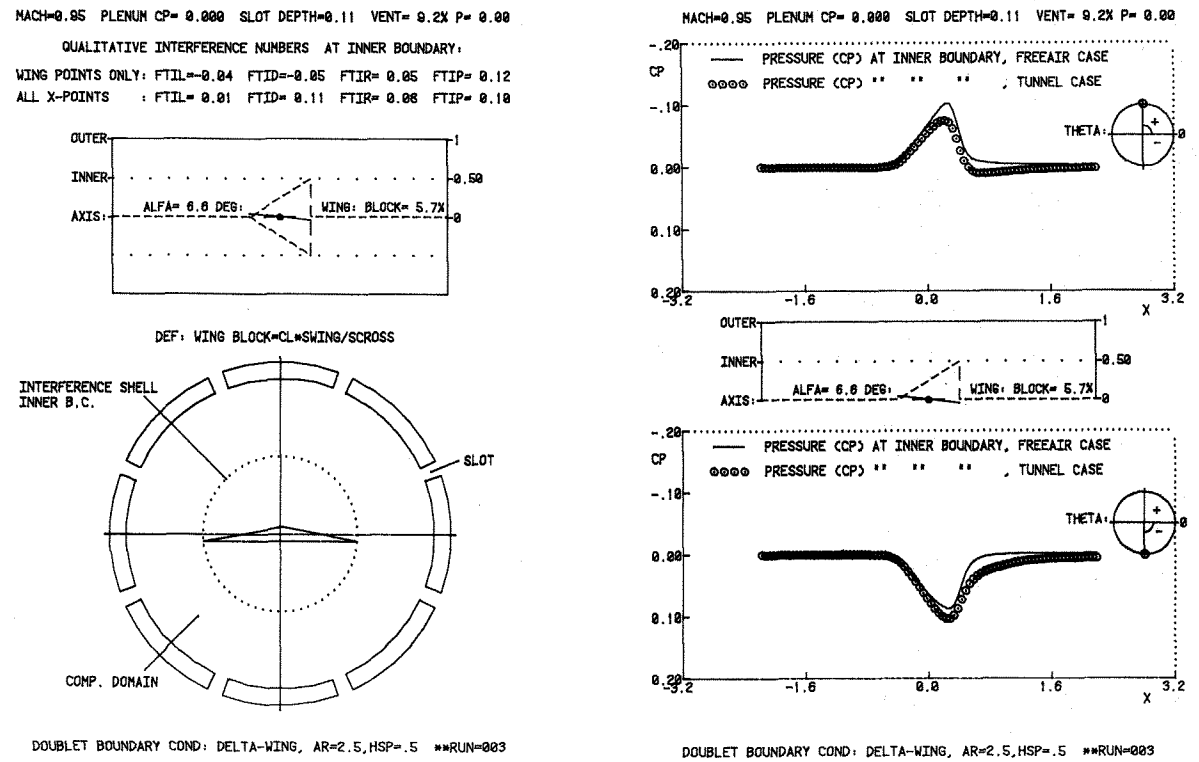

Fig 5. Pressure distributions at inner boundary of a tunnel case at M_∞=0.95, α=6.6°.

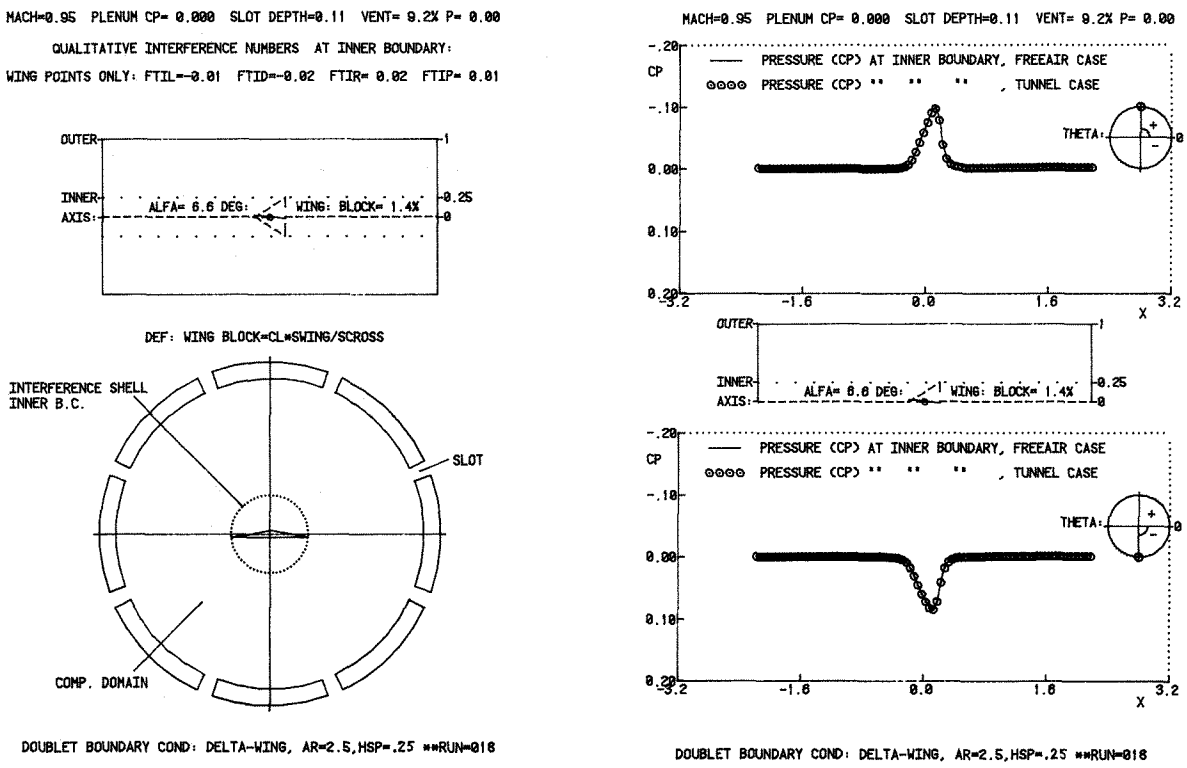

Fig 6. Pressure distributions of a small model at M_∞=0.95 and α=6.6°.

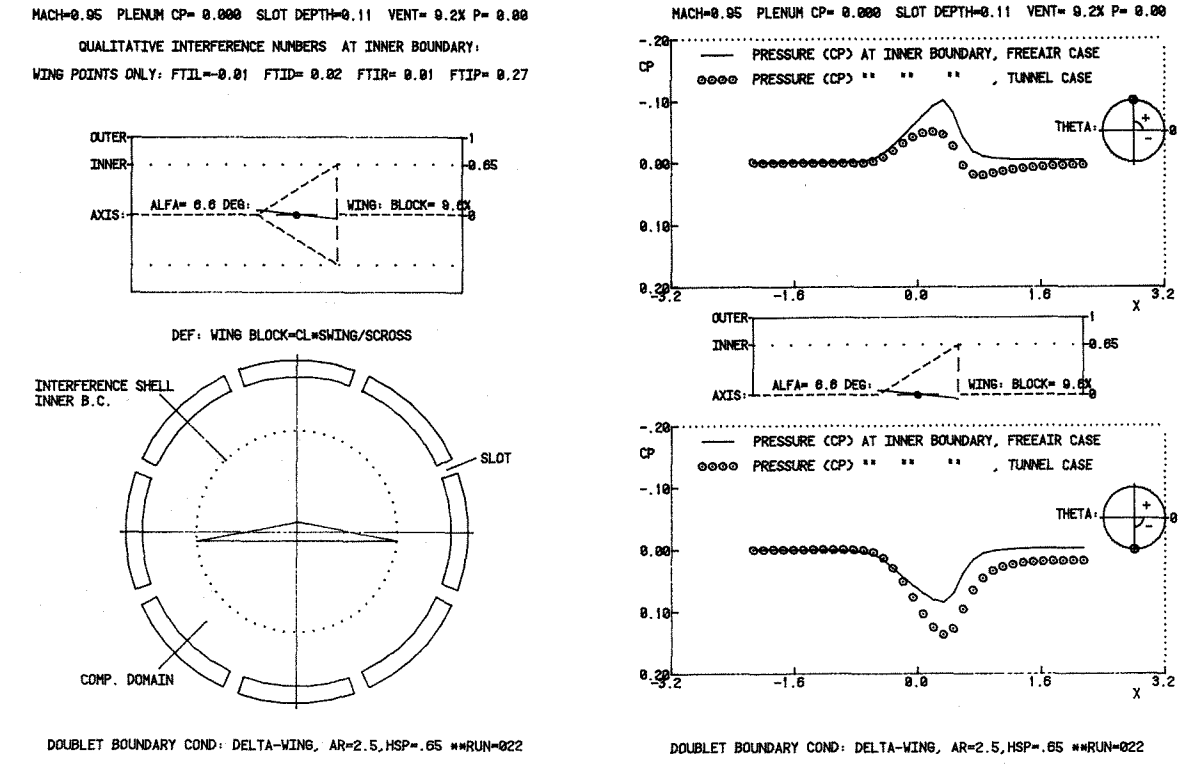

Fig 7. Pressure distributions of a large model at M_∞=0.95 and α=6.6°.

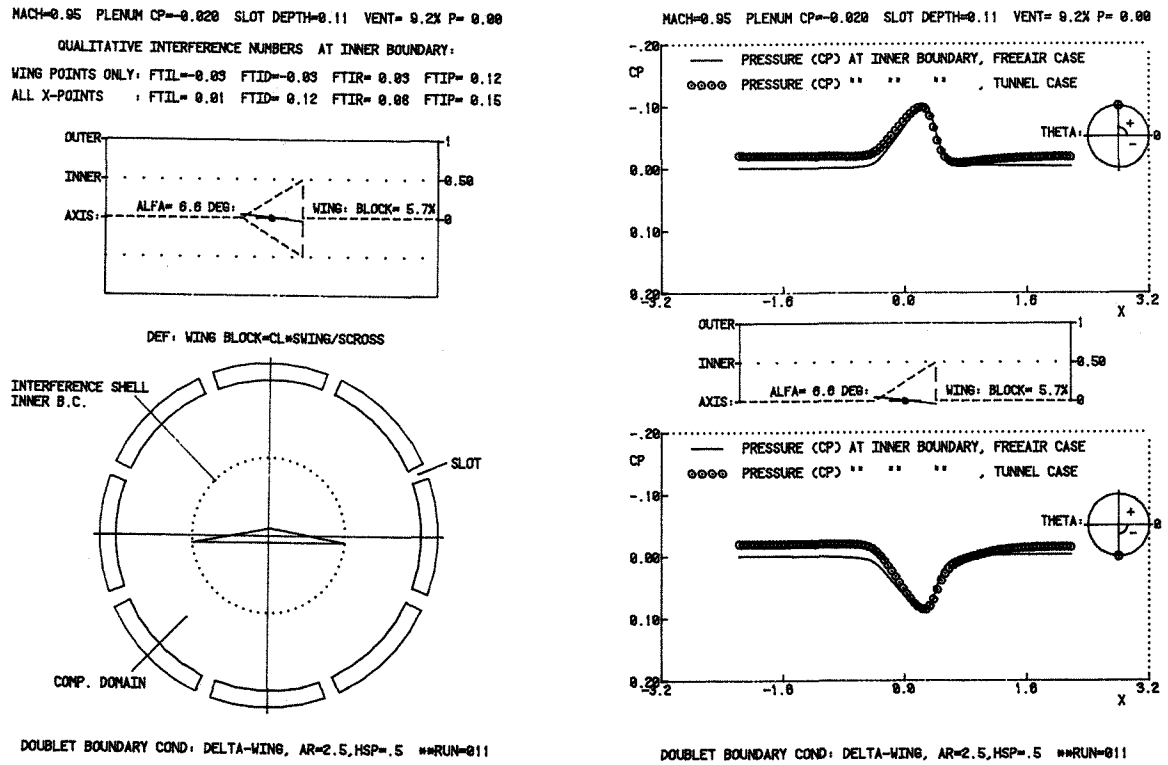

Fig 8. Pressure distributions at inner boundary for a case with plenum suction applied (M_∞=0.95, α=6.6^o)

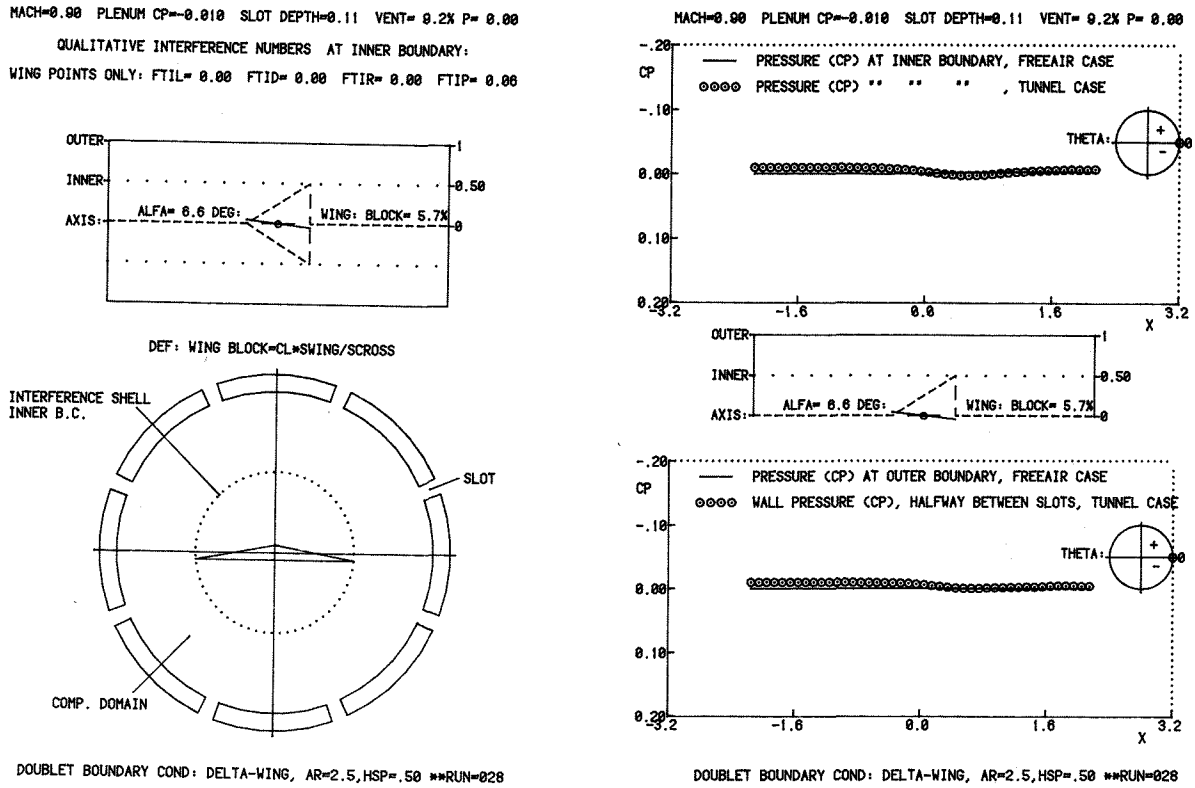

Fig 9a. Pressures and slot flow data at M_∞=0.9, α=6.6^o. Interference shell and wall pressures at θ=0^o.

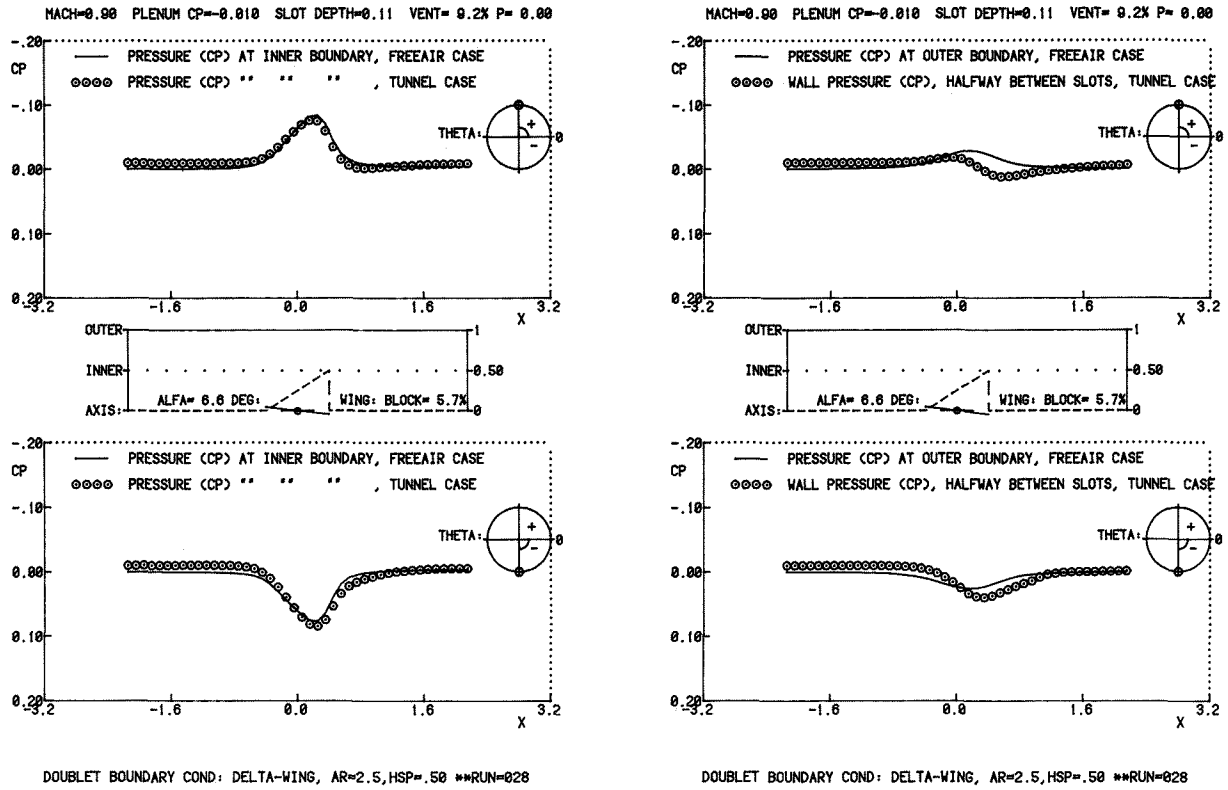

Fig 9b. Pressures and slot flow data at M_∞=0.90, α=6.6°. Interference shell and wall pressures at $\theta=\pm 90°$

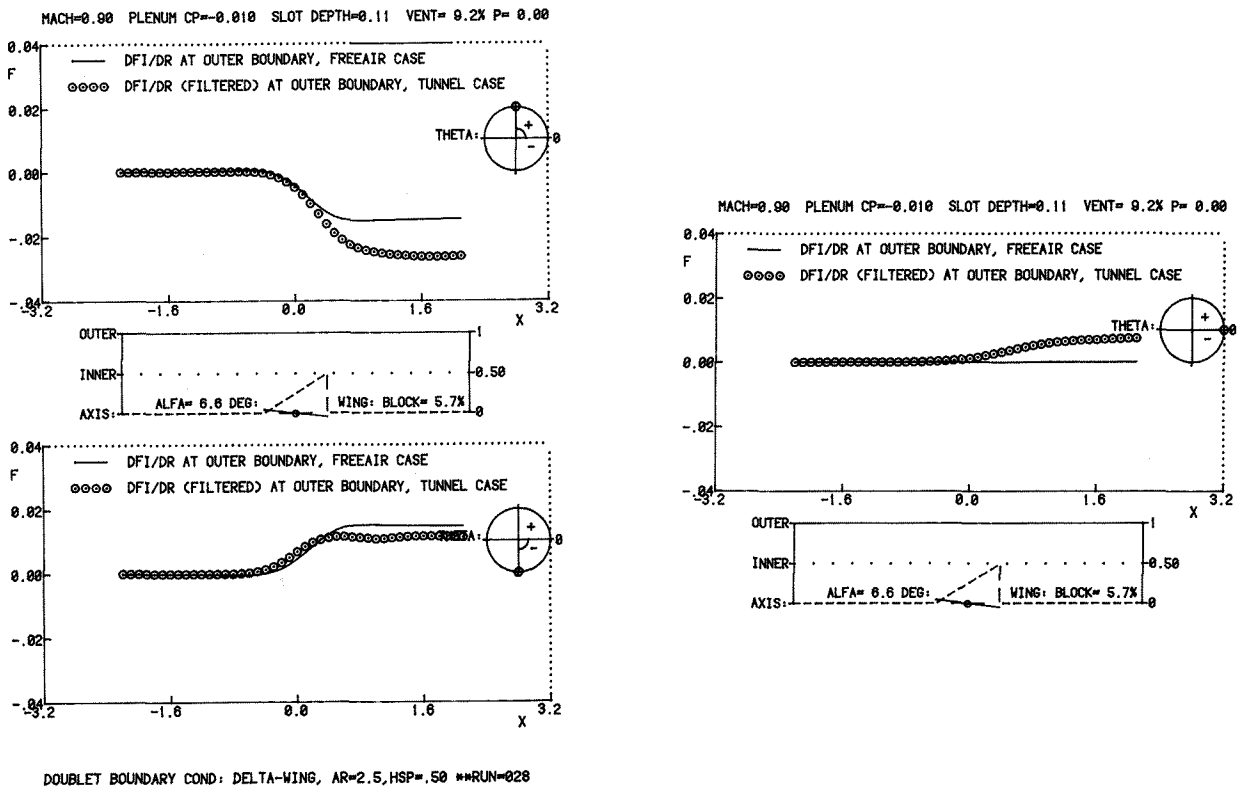

Fig 9c. Pressures and slot flow data at M_∞=0.90. α=6.6°.
Radial outflow velocities $\bar{\varphi}_r$ at wall for θ=0, $\pm 90°$

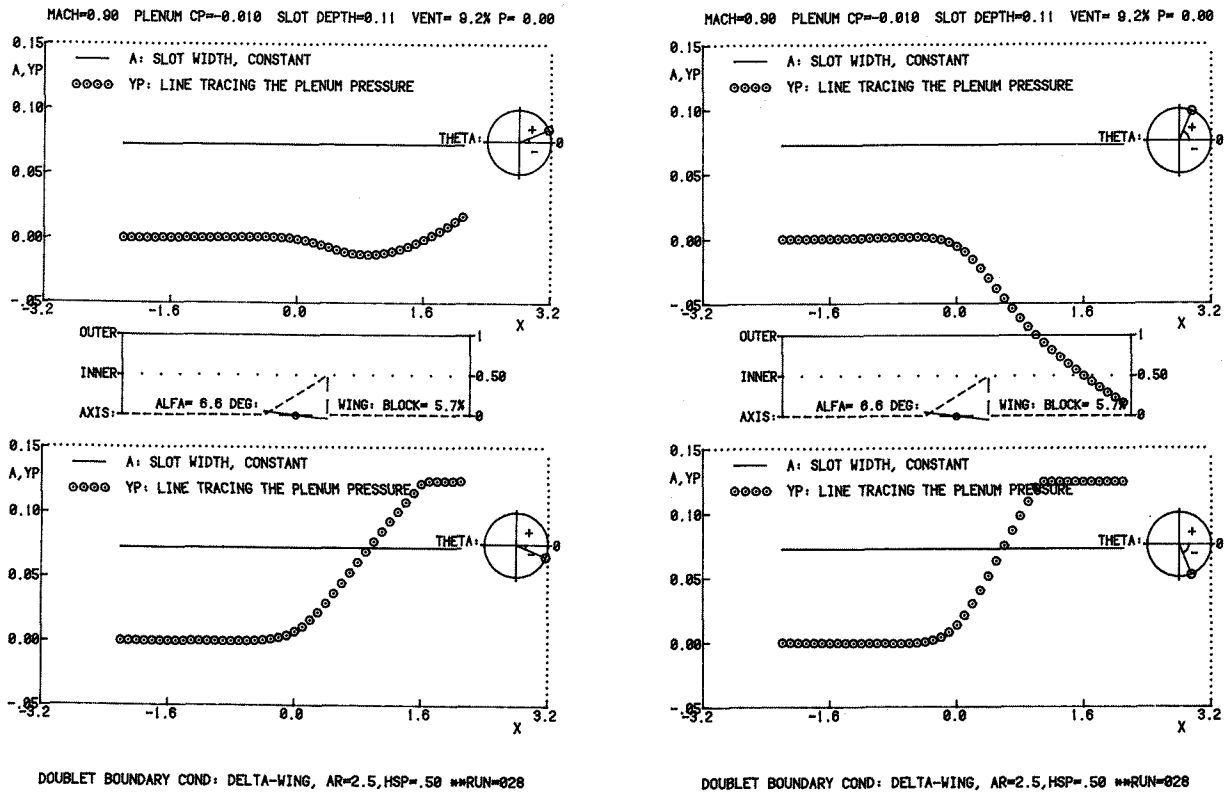

Fig 9d. Pressures and slot flow data at M_∞=0.90, α=6.6°. Slot width and plenum pressure surface positions.

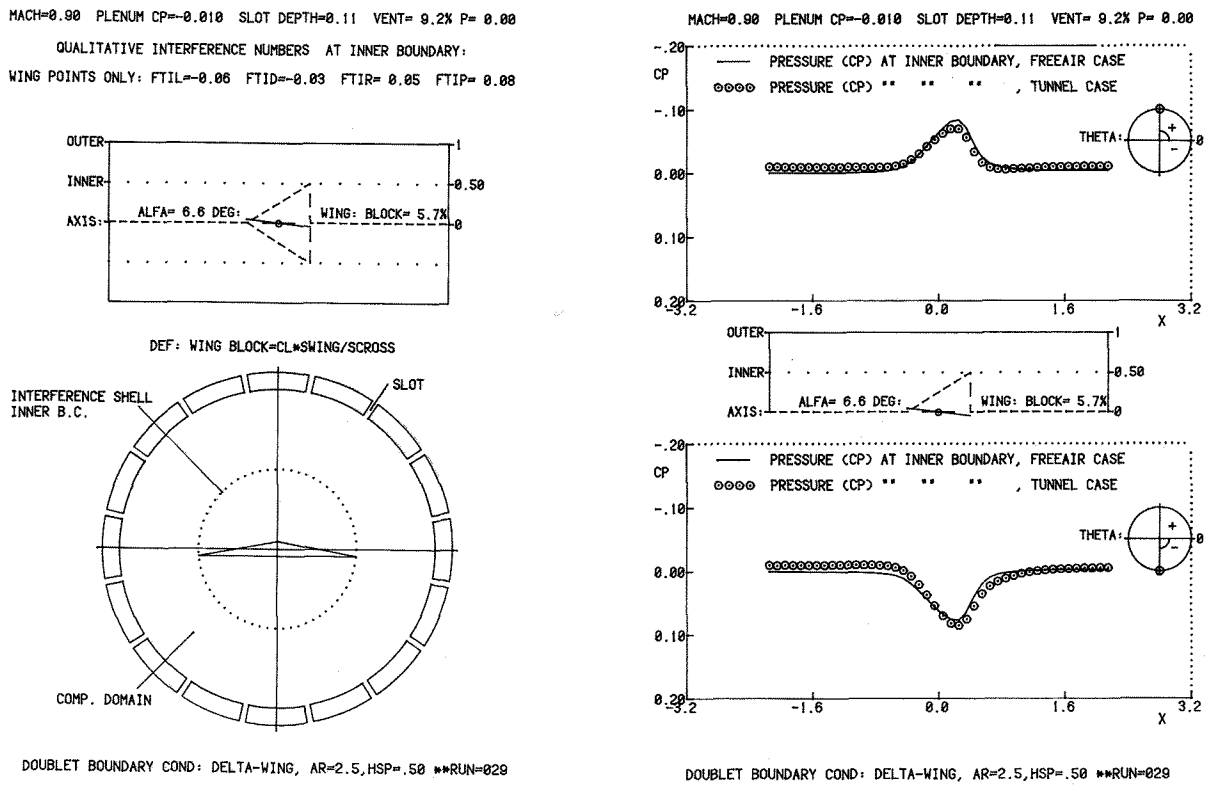

Fig 10. Pressure distributions at inner boundary when doubling the number of slots to N=16. (M_∞=0.90, α=6.6°).

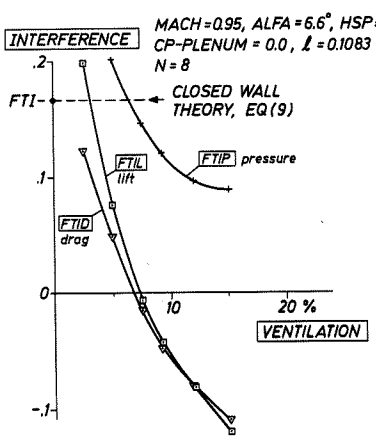

Fig 11. Wall-interference viz wall ventilation at M_∞=0.95, α=6.6°.

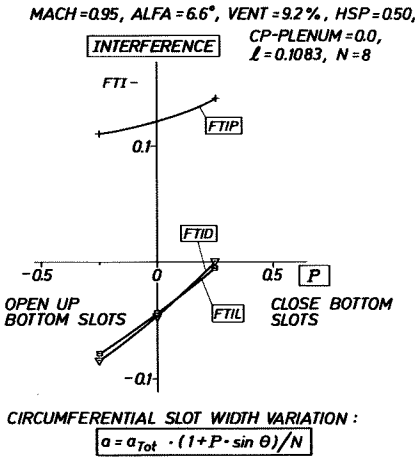

Fig 12. Wall-interference due to circumferential slot width variations at constant wall ventilation.

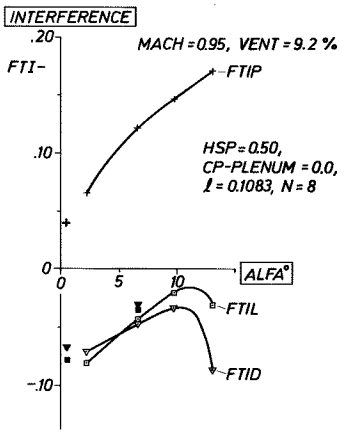

Fig 13. Wall-interference at different angles of attack.

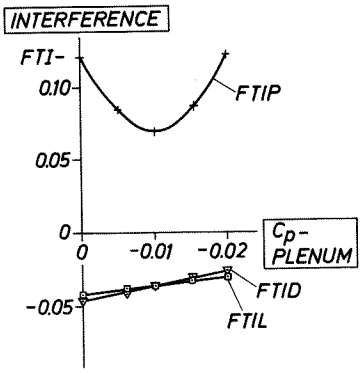

Fig 14. Interference numbers as function of plenum pressure.

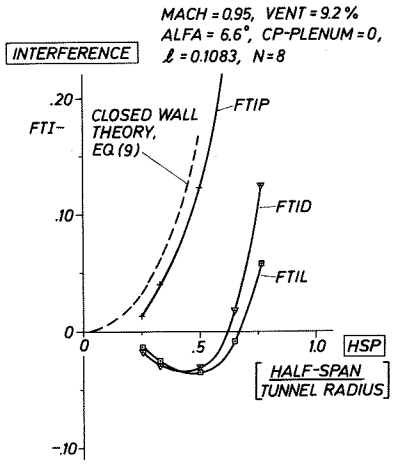

Fig 15. Interference due to model size.

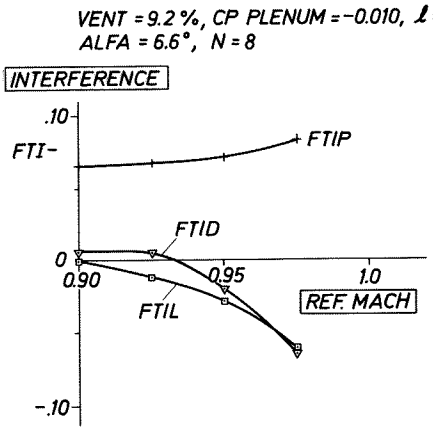

Fig 16. Mach number influence on wall-interference.